GEOLOGY | THE GEOLOGICAL SOCIETY OF AMERICA®

https://doi.org/10.1130/G54554.1

Manuscript received 20 February 2026
Revised manuscript received 3 June 2026
Manuscript accepted 23 July 2026

Published online 4 August 2026

Clumped isotopes of methane constrain the global magnitude of microbial methane oxidation in wetlands

Jiarui Liu[1,2,*], Tina Treude[1], Sebastian J.E. Krause[3], and Edward D. Young[1]

[1]Department of Earth, Planetary, and Space Sciences, University of California, Los Angeles, California 90095, USA
[2]Marine Science Institute, University of California, Santa Barbara, California 93106, USA
[3]Institute for Carbon Management, University of California, Los Angeles, California 90095, USA

ABSTRACT

Wetlands contribute one-third of global methane emissions, but the role of microbial methane consumption in regulating these emissions and their isotopologue signatures remains unclear. Here, we show that anaerobic oxidation of methane (AOM) in a coastal wetland imparts a distinct signature to the clumped isotopes of methane, characterized by a substantial positive shift in $\Delta^{13}CH_3D$ and a comparatively smaller shift in $\Delta^{12}CH_2D_2$. The consistent positive departure from the methanogenic endmember serves as a powerful tracer for cryptic methane cycling. Applying this finding to the global methane budget reveals a paradox: the globally averaged source lacks this AOM signature, and its isotopologue composition can be explained by a simple mixture of thermogenic and microbial sources. Using a Bayesian Markov Chain Monte Carlo model, we constrain the permissible global rate constants to upper limits of ~0.1–1 yr^{-1} for the anaerobic sink and ~0.1 yr^{-1} for the aerobic sink. This work develops methane clumped isotopologues as a novel tool for refining the global methane budget and presents a top-down framework to quantify the impact of microbial oxidation on global methane fluxes and their resulting atmospheric signatures.

INTRODUCTION

Methane is a potent greenhouse gas, and microbial methanogenesis in wetlands represents its largest natural source (Bridgham et al., 2013; Saunois et al., 2025). Globally, methane emissions are tracked using stable carbon ($\delta^{13}C$) and hydrogen (δD) isotope compositions, which have been used to distinguish between microbial and thermogenic sources (Whiticar, 1999; Milkov and Etiope, 2018; Michel et al., 2024; Riddell-Young et al., 2025).

The recent development of measurements of doubly substituted "clumped" isotopologues, namely $^{13}CH_3D$ and $^{12}CH_2D_2$, offers new constraints on methane formation and oxidation (Stolper et al., 2014; Wang et al., 2015; Young et al., 2017). While thermogenic methane often forms in thermodynamic equilibrium, the isotopologue compositions of methane in microbial ecosystems depend on the availability of free energy (Stolper et al., 2015; Wang et al., 2015; Douglas et al., 2020; Gropp et al., 2022; Ono et al., 2022; Mayumi et al., 2024; Liu et al., 2025b). Methanogenesis and anaerobic oxidation of methane (AOM) typically lead to distinct deviations from isotopologue equilibrium under an elevated thermodynamic driving force, whereas they tend to generate near-equilibrium isotopologue signatures under energy-limiting conditions (Ash et al., 2019; Ono et al., 2021; Giunta et al., 2022; Liu et al., 2023, 2025b; Li et al., 2025). Furthermore, at steady state, both aerobic oxidation of methane (AeOM) and photochemical oxidation by OH and Cl radicals shift $\Delta^{12}CH_2D_2$ to extremely positive values, with much smaller effects on $\Delta^{13}CH_3D$ (Haghnegahdar et al., 2017; Whitehill et al., 2017; Krause et al., 2022).

These fingerprints make clumped isotopes well suited for quantifying the impact of microbial sink processes. However, field constraints on how these signatures evolve when methanogenesis and AOM operate concurrently remain limited. We therefore investigated methane clumped isotopes in coastal wetland sediments, where active AOM allows resolution of the oxidative imprint against a relatively well-constrained methanogenic endmember, and assessed the influence of microbial oxidation on the global isotopologue budget.

STUDY AREA AND METHODOLOGY

Our study was conducted at the Carpinteria Salt Marsh Reserve in Southern California, USA (Fig. 1 and Supplemental Material[1] Fig. S1), where we selected two distinct sites characterized by active methanogenesis and AOM (Krause et al., 2025). The marine site (34°23′56.3″N, 119°32′12.0″W) is situated within the main tidal channel and exhibits a shallow sulfate-methane transition zone at ~5–20 cm, over which methane concentrations increase from ~10 to 600 μM. The hypersaline site (34°23′56.1″N, 119°32′10.2″W) is an isolated pool with lower methane concentrations (~20 μM). We sampled dissolved methane from sediment ("on-site methane") via headspace equilibration and collected sediment for laboratory incubations. Following established protocols (see the Supplemental Material), we analyzed the relative abundances of $^{13}CH_3D$ and $^{12}CH_2D_2$ using the Panorama high-mass-resolution isotope ratio mass spectrometer and reported them using the standard delta (Δ) notation, which quantifies deviations from a stochastic isotopic distribution (Young et al., 2017).

CLUMPED ISOTOPE SIGNATURES OF METHANOGENESIS IN THE SALT MARSH

In environments with high availability of free energy, methanogenesis typically produces methane with pronounced kinetic isotopologue signals (Wang et al., 2015; Gropp et al., 2022;

Jiarui Liu https://orcid.org/0000-0003-4878-6578
*jiaruiliu@ucla.edu

[1]Supplemental Material. Supplemental methods, Figures S1–S7, and Tables S1 and S2. Please visit https://doi.org/10.1130/GEOL.S.33106961 to access the supplemental material; contact editing@geosociety.org with any questions.

CITATION: Liu, J., et al., 2026, Clumped isotopes of methane constrain the global magnitude of microbial methane oxidation in wetlands: Geology, v. XX, p. , https://doi.org/10.1130/G54554.1

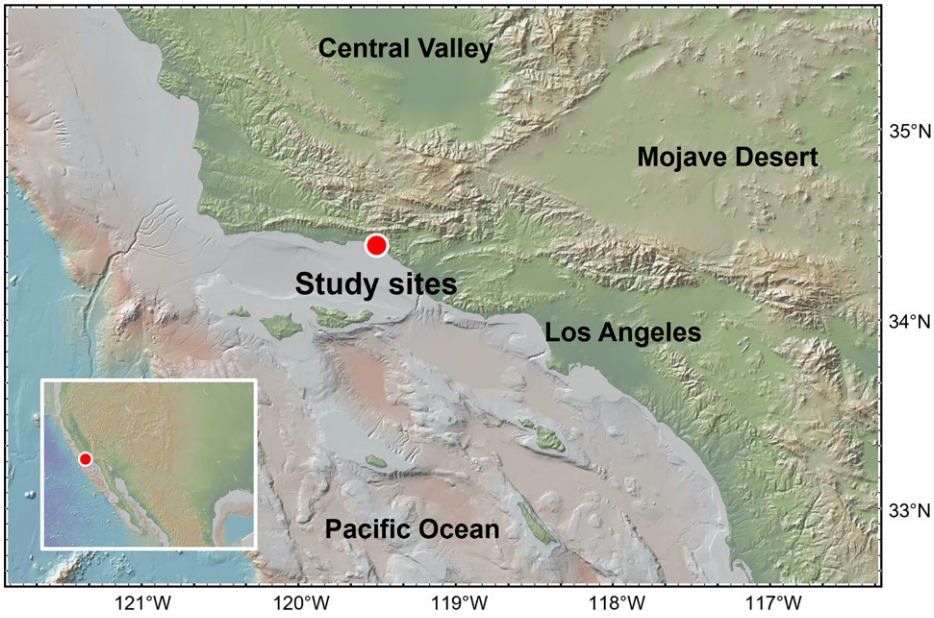

Figure 1. Location of the study sites. Map showing the Carpinteria salt marsh within the broader Southern California region, USA (GeoMapApp, www.geomapapp.org, CC BY).

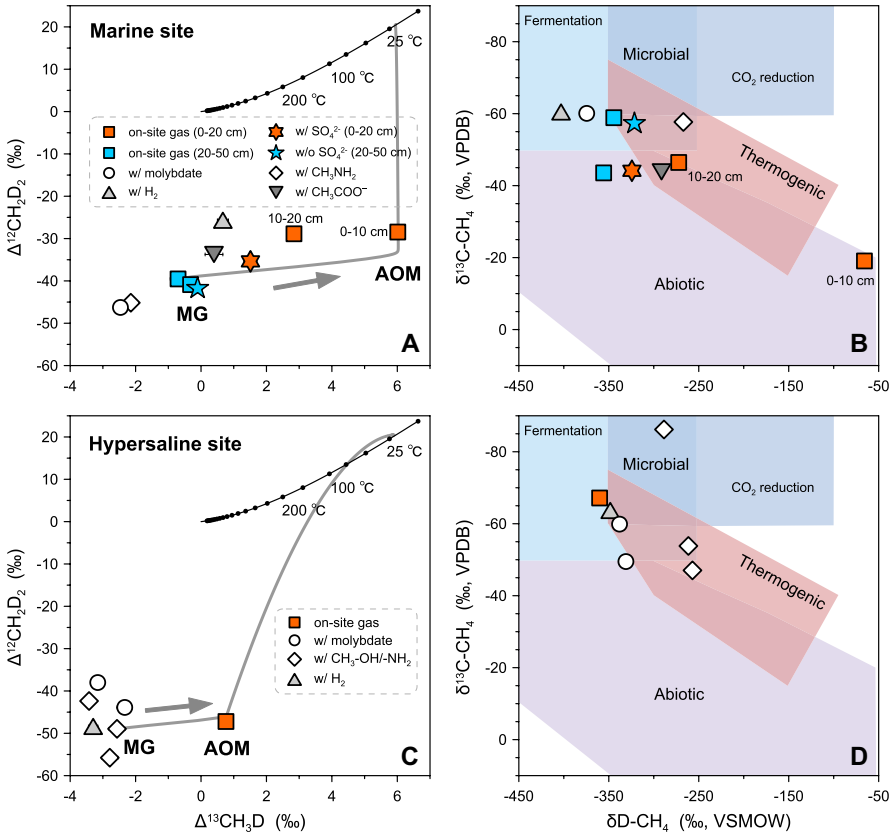

Figure 2. Methane isotopologue compositions from the Carpinteria salt marsh, California, USA. (A, C) Clumped isotopologue compositions. The solid black curve represents thermodynamic equilibrium, with corresponding temperatures indicated. (B, D) Bulk isotope compositions. Genetic fields for methane sources are from Milkov and Etiope (2018). Gray curves depict the modeled evolution of methane isotopologue compositions during concurrent methanogenesis (MG) and anaerobic oxidation of methane (AOM; Liu et al., 2023). The curvature of the modeled trajectory is primarily controlled by the reaction reversibility, which was adjusted to fit the data, while the ratio of methane production to oxidation rates does not affect the model output in the high-reversibility regime (Fig. S3; see text footnote 1). Error bars representing 1 SE are mostly encompassed by individual data points. Unless specified, the sediment depth for both sites is 0–20 cm. VPDB—Vienna Peedee belemnite; VSMOW—Vienna standard mean ocean water.

Li et al., 2025; Liu et al., 2025b). Consistent with this expectation, methane at the marine site exhibits strong isotopologue disequilibrium, defined here as deviations from thermodynamic equilibrium (black curve in Fig. 2A). On-site methane from below the sulfate-methane transition zone, as well as methane from sulfate-free sediment incubations, yield highly negative $\Delta^{13}CH_3D$ and $\Delta^{12}CH_2D_2$ values, as low as −0.7‰ and −41.8‰, respectively, indicative of disequilibrium methane formation.

We conducted laboratory slurry incubations of surface sediments from the marine site to investigate the clumped isotope signatures of the three major methanogenic pathways: hydrogenotrophic, acetoclastic, and methylotrophic (see section 2 of the Supplemental Material). In experiments where we inhibited AOM coupled to sulfate and iron reduction (using molybdate and sulfide, respectively), these inhibitors also blocked organoclastic sulfate and iron reduction, which eliminated competition with methanogenesis for hydrogen and acetate. While this was expected to promote hydrogenotrophic and acetoclastic pathways, the methane produced exhibited a clumped isotope signature nearly identical to that from incubations amended with methylamine, a substrate for methylotrophic methanogenesis (Fig. 2A). This indicates that methylotrophic methanogenesis predominated in surface sediments. In parallel, incubations amended with H_2 and acetate yielded methane with more positive $\Delta^{13}CH_3D$ and $\Delta^{12}CH_2D_2$ values, suggesting that the hydrogenotrophic and acetoclastic pathways become significant only when substrates are abundant.

At the sulfate-rich hypersaline site, methanogenesis is dominated by the methylotrophic pathway (Oremland and Polcin, 1982; Krause et al., 2025). Incubations amended with various methylated substrates or AOM inhibitors produced methane with strongly negative $\Delta^{13}CH_3D$ and $\Delta^{12}CH_2D_2$ values (Fig. 2C), similar to those observed at the marine site, confirming that active methanogenesis in both environments generates a distinct disequilibrium signature.

CONCURRENT METHANOGENESIS AND ANAEROBIC OXIDATION OF METHANE

While incubations primarily reflect methanogenic signals, on-site surface methane integrates concurrent methanogenesis and AOM. At the marine site, high rates of sulfate reduction and AOM were observed in the upper 20 cm of sediment, largely fueled by upward methane transport from the deeper methanogenic zone (Fig. S2; Krause et al., 2025). This sulfate-driven AOM left a distinct imprint on the dissolved methane pool. Compared with the negative values in the methanogenic zone (blue symbols in Fig. 2A), $\Delta^{13}CH_3D$ values increased progressively toward the sediment surface, reaching

+2.8‰ (10−20 cm) and +6.0‰ (0−10 cm) (Fig. 2A). A similar, albeit comparatively smaller, positive shift was observed for the $\Delta^{12}CH_2D_2$ values. The highest measured $\Delta^{13}CH_3D$ value of 6.0‰ ± 0.2‰ approaches the equilibrium value expected near ambient temperature, whereas $\Delta^{12}CH_2D_2$ remains far from equilibrium, indicating partial isotopologue equilibration during AOM. A similar positive departure from baseline methanogenic values was also observed in sulfate-rich sediment incubations.

A similar shift occurred at the hypersaline site, despite a different dominant electron acceptor, iron(III) (Fig. 2C). At this site, low methane concentrations are maintained by cryptic methane cycling (Figs. S2D and S2E), a process where methylotrophic methanogenesis fuels AOM that is coupled primarily to iron oxide reduction (Liu et al., 2025a). This process drove an increase in the on-site $\Delta^{13}CH_3D$ value of 3.7‰ in the upper 20 cm relative to the methanogenic endmember.

We adapted the model from Liu et al. (2023) to simulate the evolution of methane isotopologues during concurrent production and consumption. The model evolves from the methanogenic endmember toward full equilibrium and successfully reproduces the empirical data by adjusting the reversibility of the reaction, showing a significant positive shift in $\Delta^{13}CH_3D$ and a comparatively smaller one in $\Delta^{12}CH_2D_2$ (Figs. 2 and S3). While our results at Carpinteria reflect a state of partial equilibrium, AOM in other settings could drive the isotopologue compositions toward complete equilibrium or beyond it through kinetic fractionation (Ash et al., 2019; Liu et al., 2023). The specific isotopic trajectory likely depends on environmental factors such as substrate concentration, biomass density, and the overall thermodynamic drive, all of which vary across diverse global wetland regions.

Regardless of the final isotopologue state, our findings confirm that AOM consistently drives a positive departure from the methanogenic endmember (Giunta et al., 2022; Liu et al., 2023). In contrast, traditional bulk isotopes are less reliable for tracking AOM because variable electron-acceptor availability and the resulting changes in AOM reversibility can drive either enrichment or depletion in methane $\delta^{13}C$ and δD, with the observed direction also depending on the isotopic compositions of carbon and hydrogen sources and the initial methane composition (Figs. 2B and 2D; Wegener et al., 2021; Liu et al., 2023). This makes clumped isotopes a unique and powerful tool for tracking cryptic methane cycling, especially in environments where direct rate measurements are impractical.

IMPLICATIONS FOR THE GLOBAL METHANE BUDGET

The isotopologue signatures of methane production and oxidation characterized in this study have direct implications for the global methane budget. We assess these by first constraining the clumped isotopologue compositions of the primary global methane sources using a compilation of published data (Fig. 3; Defratyka et al., 2025). The two major source categories in our simplified mixing model are thermogenic methane and microbial methane from surface environments with high free-energy availability (e.g., wetlands, lakes, and agriculture), assuming that microbial methane produced under energy limitation from terrestrial subsurface environments (e.g., hydrocarbon biodegradation) contributes less directly to atmospheric emissions. Although our endmember estimates, particularly for high-energy microbial methane, carry uncertainties due to natural variability (e.g., Lalk et al., 2024; Sun et al., 2025; Wang et al., 2026), this simple classification scheme allows us to infer the relative contributions of various global methane sources to the atmosphere. The inferred isotopologue composition of the total global methane source, calculated from atmospheric methane using non-steady-state models (Chung and Arnold, 2021; Haghnegahdar et al., 2023; Sivan et al., 2024), plots directly on mixing lines between the thermogenic and microbial endmembers (Fig. 3). This simplified mixing model indicates that microbial methanogenesis contributes ~80%–90% of global methane emissions, near the upper end of previous estimates (55%–85%; Schwietzke et al., 2016; Saunois et al., 2025). While this estimate remains subject to uncertainties in source classification and microbial endmember compositions, it provides a valuable independent constraint that can be refined with future data on microbial sources.

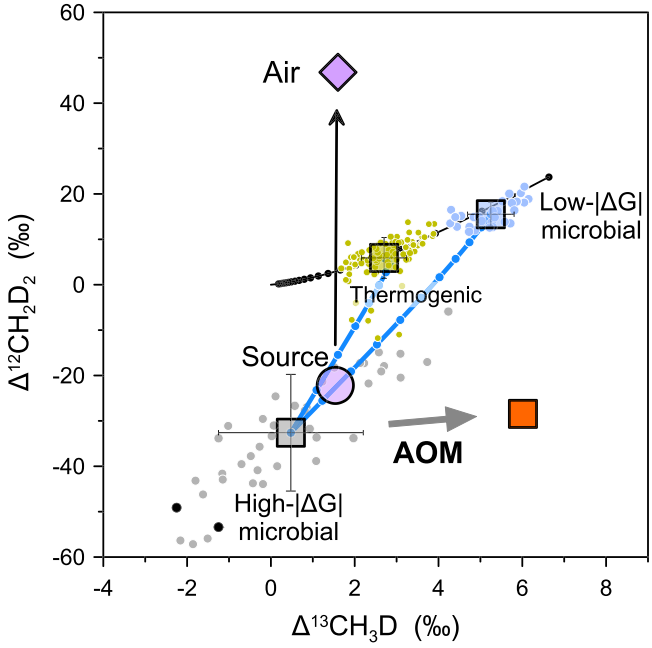

Figure 3. Schematic illustration of the global methane budget in clumped isotopologue space. The plot displays the average compositions of major methane sources, atmospheric methane, and the derived total source. (1) Source endmembers (squares): average compositions for thermogenic, high-energy microbial, and low-energy microbial methane from terrestrial environments. Plotted literature data were compiled by Defratyka et al. (2025). Data from two brackish sites at the Carpinteria salt marsh (California, USA) are shown as black dots (Liu et al., 2025b), plotting within the high-energy microbial field. (2) Atmosphere and total source (diamonds and circles): the purple diamond represents measured atmospheric methane, and the purple circle is the calculated total global source from a non-steady-state model (from Haghnegahdar et al., 2023). The black arrow illustrates the fractionation trajectory of photochemical methane oxidation in the atmosphere. (3) Mixing model (blue lines): the curves are two-component mixing lines between endmembers, with points marking 10% intervals. (4) This study (orange square): the orange square shows on-site methane from our study that carries an anaerobic oxidation of methane (AOM) signature. The gray arrow illustrates the conceptual trajectory of AOM originating from the high-energy microbial field.

Although the total global average contributions of microbial and thermogenic gases to the atmosphere are indicated by a simple mixing model in methane isotopologue space, it is important to acknowledge the crucial role of microbial oxidation in mitigating methane emissions. To investigate the impact of microbial oxidation on atmospheric methane isotopologues, we developed a time-dependent two-box model (see section 5 of the Supplemental Material). This model simulates the evolution of methane isotopologues in the atmosphere and the surface microbial environment from 1984 to 2024. We used a Bayesian Markov Chain Monte Carlo inversion to determine the maximum permissible rate constants for AeOM and AOM losses within the surface microbial environment that best accommodate modern atmospheric measurements (Figs. 4 and S4).

The posterior distribution for k_{AeOM} shows a sharp decline in probability density above 10^{-1} yr^{-1}, indicating a global upper bound comparable to the atmospheric OH oxidation rate constant. In contrast, constraints on k_{AOM} depend strongly on the assumed isotopologue fraction-

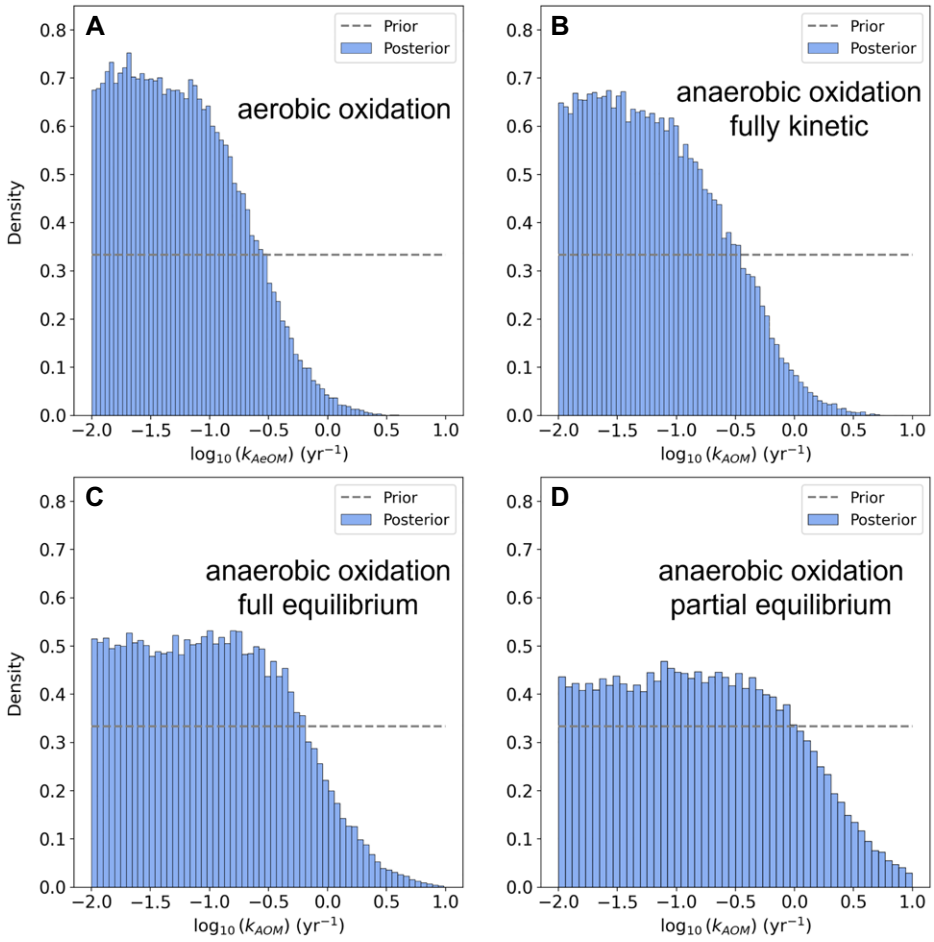

Figure 4. Posterior probability distributions for the global rate constants of aerobic and anaerobic methane oxidation, shown in comparison with their respective uniform prior distributions within the two-box model. Due to the high reversibility of anaerobic oxidation of methane (AOM), we evaluate three representative scenarios with varying isotopologue fractionation factors: fully kinetic, full equilibrium, and partial equilibrium.

ation mechanism. Under a fully kinetic fractionation scenario, k_{AOM} is similarly restricted to $\sim 10^{-1}$ yr^{-1}. If full equilibrium fractionation dominates, the allowable upper limit increases to $\sim 10^{-0.5}$ yr^{-1}. When partial equilibrium effects consistent with our site observations are incorporated, k_{AOM} values approaching $\sim 10^{0}$ yr^{-1} remain permissible. Across these scenarios, the global methane budget constrains the upper limit of k_{AOM} to ~0.1–1 yr^{-1} for the smaller and more uncertain surface microbial methane reservoir. While global clumped isotope effects of AOM and several model priors remain subject to uncertainties that will be refined through future investigations, methane isotopologues provide a powerful framework for quantifying microbial filters and their global impact.

CONCLUSIONS

This study demonstrates that concurrent methanogenesis and AOM, commonly referred to as cryptic methane cycling, impart a distinct signature on the clumped isotopologue compositions of methane in a coastal wetland. This signature is characterized by a large positive shift in $\Delta^{13}CH_3D$ relative to a smaller shift in $\Delta^{12}CH_2D_2$. The consistent positive departure from the methanogenic endmember can be driven by either kinetic or equilibrium isotope effects, providing a unique tool for tracking cryptic methane cycling.

By integrating these isotopic signatures into a global two-box model, we demonstrate that a top-down approach can constrain the maximum rate constants of global microbial filters. Unlike bottom-up methods requiring aggregation of local oxidation rates, this atmospheric inversion defines permissible ranges of up to ~0.1 yr^{-1} for the global aerobic sink and ~0.1–1 yr^{-1} for the global anaerobic sink. Ultimately, this framework allows us to quantify the global capacity for microbial methane mitigation, bridging the gap between site-specific observations and global atmospheric trends.

ACKNOWLEDGMENTS

This research was supported by the NASA FINESST (Future Investigators in NASA Earth and Space Science and Technology) Fellowship 80NSSC21K1529, National Science Foundation grant EAR-1852912, and NASA grant 80NSSC21K0477. We thank the University of California Natural Reserve System and A. Brooks for authorization for field sampling. We are grateful to G. Vetushko, J. Labidi, R. Ambrose, D. Robinson, M. Hasnain, E. Lim, D.J. Yousavich, T. Holzmann, B. Cloutier, M. Lin, M. Puls, and S. Lenkin for assistance. We also thank the anonymous reviewers for their helpful and constructive reviews of this paper.

REFERENCES CITED

Ash, J.L., Egger, M., Treude, T., Kohl, I., Cragg, B., Parkes, R.J., Slomp, C.P., Sherwood Lollar, B., and Young, E.D., 2019, Exchange catalysis during anaerobic methanotrophy revealed by $^{12}CH_2D_2$ and $^{13}CH_3D$ in methane: Geochemical Perspectives Letters, v. 10, p. 26–30, https://doi.org/10.7185/geochemlet.1910.

Bridgham, S.D., Cadillo-Quiroz, H., Keller, J.K., and Zhuang, Q., 2013, Methane emissions from wetlands: Biogeochemical, microbial, and modeling perspectives from local to global scales: Global Change Biology, v. 19, p. 1325–1346, https://doi.org/10.1111/gcb.12131.

Chung, E., and Arnold, T., 2021, Potential of clumped isotopes in constraining the global atmospheric methane budget: Global Biogeochemical Cycles, v. 35, https://doi.org/10.1029/2020GB006883.

Defratyka, S.M., et al., 2025, Global inventory of doubly substituted isotopologues of methane ($\Delta^{13}CH_3D$ and $\Delta^{12}CH_2D_2$): Earth System Science Data, v. 17, p. 6889–6910, https://doi.org/10.5194/essd-17-6889-2025.

Douglas, P.M.J., et al., 2020, Clumped isotopes link older carbon substrates with slower rates of methanogenesis in northern lakes: Geophysical Research Letters, v. 47, https://doi.org/10.1029/2019GL086756.

Giunta, T., Young, E.D., Labidi, J., Sansjofre, P., Jézéquel, D., Donval, J.-P., Brandily, C., and Ruffine, L., 2022, Extreme methane clumped isotopologue bio-signatures of aerobic and anaerobic methanotrophy: Insights from the Lake Pavin and the Black Sea sediments: Geochimica et Cosmochimica Acta, v. 338, p. 34–53, https://doi.org/10.1016/j.gca.2022.09.034.

Gropp, J., Jin, Q., and Halevy, I., 2022, Controls on the isotopic composition of microbial methane: Science Advances, v. 8, https://doi.org/10.1126/sciadv.abm5713.

Haghnegahdar, M.A., Schauble, E.A., and Young, E.D., 2017, A model for $^{12}CH_2D_2$ and $^{13}CH_3D$ as complementary tracers for the budget of atmospheric CH_4: Global Biogeochemical Cycles, v. 31, p. 1387–1407, https://doi.org/10.1002/2017GB005655.

Haghnegahdar, M.A., et al., 2023, Tracing sources of atmospheric methane using clumped isotopes: Proceedings of the National Academy of Sciences of the United States of America, v. 120, https://doi.org/10.1073/pnas.2305574120.

Krause, S.J.E., Liu, J., Young, E.D., and Treude, T., 2022, $\Delta^{13}CH_3D$ and $\Delta^{12}CH_2D_2$ signatures of methane aerobically oxidized by *Methylosinus trichosporium* with implications for deciphering the provenance of methane gases: Earth and Planetary Science Letters, v. 593, https://doi.org/10.1016/j.epsl.2022.117681.

Krause, S.J.E., Wipfler, R., Liu, J., Yousavich, D.J., Robinson, D., Hoyt, D.W., Orphan, V.J., and Treude, T., 2025, Spatial evidence of cryptic methane cycling and methylotrophic metabolisms along a land–ocean transect in salt marsh sediment: Geochimica et Cosmochimica Acta,

v. 404, p. 53–71, https://doi.org/10.1016/j.gca.2025.07.019.

Lalk, E., Velez, A., and Ono, S., 2024, Methane clumped isotopologue variability from ebullition in a mid-latitude lake: ACS Earth & Space Chemistry, v. 8, p. 689–701, https://doi.org/10.1021/acsearthspacechem.3c00282.

Li, J., et al., 2025, The clumped isotope signatures of multiple methanogenic metabolisms: Environmental Science & Technology, v. 59, p. 13,798–13,810, https://doi.org/10.1021/acs.est.5c03255.

Liu, J., et al., 2023, Reversibility controls on extreme methane clumped isotope signatures from anaerobic oxidation of methane: Geochimica et Cosmochimica Acta, v. 348, p. 165–186, https://doi.org/10.1016/j.gca.2023.02.022.

Liu, J., Klonicki-Ference, E., Krause, S.J.E., and Treude, T., 2025a, Iron oxides fuel anaerobic oxidation of methane in the presence of sulfate in hypersaline coastal wetland sediment: Environmental Science & Technology, v. 59, p. 513–522, https://doi.org/10.1021/acs.est.4c10639.

Liu, J., et al., 2025b, Clumped isotopes of methane trace bioenergetics in the environment: Science Advances, v. 11, https://doi.org/10.1126/sciadv.adu1401.

Mayumi, D., et al., 2024, Hydrogenotrophic methanogens overwrite isotope signals of subsurface methane: Science, v. 386, p. 1372–1376, https://doi.org/10.1126/science.ado0126.

Michel, S.E., et al., 2024, Rapid shift in methane carbon isotopes suggests microbial emissions drove record high atmospheric methane growth in 2020–2022: Proceedings of the National Academy of Sciences of the United States of America, v. 121, https://doi.org/10.1073/pnas.2411212121.

Milkov, A.V., and Etiope, G., 2018, Revised genetic diagrams for natural gases based on a global dataset of >20,000 samples: Organic Geochemistry, v. 125, p. 109–120, https://doi.org/10.1016/j.orggeochem.2018.09.002.

Ono, S., Rhim, J.H., Gruen, D.S., Taubner, H., Kölling, M., and Wegener, G., 2021, Clumped isotopologue fractionation by microbial cultures performing the anaerobic oxidation of methane: Geochimica et Cosmochimica Acta, v. 293, p. 70–85, https://doi.org/10.1016/j.gca.2020.10.015.

Ono, S., Rhim, J.H., and Ryberg, E.C., 2022, Rate limits and isotopologue fractionations for microbial methanogenesis examined with combined pathway protein cost and isotopologue flow network models: Geochimica et Cosmochimica Acta, v. 325, p. 296–315, https://doi.org/10.1016/j.gca.2022.03.017.

Oremland, R.S., and Polcin, S., 1982, Methanogenesis and sulfate reduction: Competitive and noncompetitive substrates in estuarine sediments: Applied and Environmental Microbiology, v. 44, p. 1270–1276, https://doi.org/10.1128/aem.44.6.1270-1276.1982.

Riddell-Young, B., et al., 2025, Microbial driver of 2006–2023 CH_4 growth indicated by trends in atmospheric $\delta D–CH_4$ and $\delta^{13}C–CH_4$: Proceedings of the National Academy of Sciences of the United States of America, v. 122, https://doi.org/10.1073/pnas.2516543122.

Saunois, M., et al., 2025, Global methane budget 2000–2020: Earth System Science Data, v. 17, p. 1873–1958, https://doi.org/10.5194/essd-17-1873-2025.

Schwietzke, S., et al., 2016, Upward revision of global fossil fuel methane emissions based on isotope database: Nature, v. 538, p. 88–91, https://doi.org/10.1038/nature19797; erratum available at https://doi.org/10.1038/nature21422.

Sivan, M., Röckmann, T., van der Veen, C., and Popa, M.E., 2024, Extraction, purification, and clumped isotope analysis of methane ($\Delta^{13}CDH_3$ and $\Delta^{12}CD_2H_2$) from sources and the atmosphere: Atmospheric Measurement Techniques, v. 17, p. 2687–2705, https://doi.org/10.5194/amt-17-2687-2024.

Stolper, D.A., et al., 2014, Formation temperatures of thermogenic and biogenic methane: Science, v. 344, p. 1500–1503, https://doi.org/10.1126/science.1254509.

Stolper, D.A., Martini, A.M., Clog, M., Douglas, P.M., Shusta, S.S., Valentine, D.L., Sessions, A.L., and Eiler, J.M., 2015, Distinguishing and understanding thermogenic and biogenic sources of methane using multiply substituted isotopologues: Geochimica et Cosmochimica Acta, v. 161, p. 219–247, https://doi.org/10.1016/j.gca.2015.04.015.

Sun, J., Magen, C., Haghnegahdar, M.A., Liu, J., Fernandez, J.M., and Farquhar, J., 2025, Constraining wetland and landfill methane emission signatures through atmospheric methane clumped isotopologue measurements: Journal of Geophysical Research: Biogeosciences, v. 130, https://doi.org/10.1029/2024JG008249.

Wang, D.T., et al., 2015, Nonequilibrium clumped isotope signals in microbial methane: Science, v. 348, p. 428–431, https://doi.org/10.1126/science.aaa4326.

Wang, X., et al., 2026, Clumped isotopes tracing methane cycle and budget: A review: Earth-Science Reviews, v. 272, https://doi.org/10.1016/j.earscirev.2025.105349.

Wegener, G., Gropp, J., Taubner, H., Halevy, I., and Elvert, M., 2021, Sulfate-dependent reversibility of intracellular reactions explains the opposing isotope effects in the anaerobic oxidation of methane: Science Advances, v. 7, https://doi.org/10.1126/sciadv.abe4939.

Whitehill, A.R., Joelsson, L.M.T., Schmidt, J.A., Wang, D.T., Johnson, M.S., and Ono, S., 2017, Clumped isotope effects during OH and Cl oxidation of methane: Geochimica et Cosmochimica Acta, v. 196, p. 307–325, https://doi.org/10.1016/j.gca.2016.09.012.

Whiticar, M.J., 1999, Carbon and hydrogen isotope systematics of bacterial formation and oxidation of methane: Chemical Geology, v. 161, p. 291–314, https://doi.org/10.1016/S0009-2541(99)00092-3.

Young, E.D., et al., 2017, The relative abundances of resolved $^{12}CH_2D_2$ and $^{13}CH_3D$ and mechanisms controlling isotopic bond ordering in abiotic and biotic methane gases: Geochimica et Cosmochimica Acta, v. 203, p. 235–264, https://doi.org/10.1016/j.gca.2016.12.041.

Printed in the USA